



# Comparison of the WRF and HARMONIE models ability for mountain wave warnings

J. Díaz-Fernández<sup>a,\*</sup>, P. Bolgiani<sup>a</sup>, D. Santos-Muñoz<sup>b</sup>, L. Quitián-Hernández<sup>a,c</sup>, M. Sastre<sup>a</sup>, F. Valero<sup>a,d</sup>, J.I. Farrán<sup>c</sup>, J.J. González-Alemán<sup>a</sup>, M.L. Martín<sup>c,d</sup>

<sup>a</sup> Department of Earth Physics and Astrophysics, Faculty of Physics, Complutense University of Madrid, Madrid, Spain

<sup>b</sup> Danmarks Meteorologiske Institut, Copenhagen, Denmark

<sup>c</sup> Department of Applied Mathematics, Faculty of Computer Engineering, University of Valladolid, Segovia, Spain

<sup>d</sup> Institute of Interdisciplinary Mathematics (IMI), Complutense University of Madrid, Madrid, Spain

## ARTICLE INFO

### Keywords:

Mountain lee waves

Icing

Lenticular clouds

WRF

HARMONIE

Warning

Decision tree

## ABSTRACT

Mountain lee waves usually involve aircraft icing and turbulence events. These weather phenomena, in turn, are a threat to aviation safety. For this reason, mountain lee waves are an interesting subject of study for the scientific community. This paper analyses several mountain lee waves events in the south-east of the Guadarrama mountain range, near the Adolfo Suarez Madrid-Barajas airport (Spain), using the Weather Research and Forecasting (WRF) and the HARMONIE-AROME high-resolution numerical models. For this work, simulated brightness temperature from the optimum WRF parametrization schemes and from the HARMONIE are validated using satellite observations to evaluate the performance of the models in reproducing the lenticular clouds associated to mountain lee waves. The brightness temperature probability density shows interesting differences between both models. Following, a mountain wave characterization is performed simulating some atmospheric variables (wind direction, wind speed, atmospheric stability, liquid water content and temperature) in several grid points located in the leeward, windward and over the summit of the mountains. The characterization results are compared for both numerical models and a decision tree is developed for each to forecast and warn the mountain lee waves, lenticular clouds and icing events with a 24 to 48 h lead time. These warnings are validated using several skill scores, revealing similar results for both models.

## 1. Introduction

Meteorological phenomena have a great influence in human activities, particularly in aviation, as for this mean of transportation in intrinsically connected with the troposphere, where the adverse meteorological phenomena occur. Turbulence and aircraft icing conditions related to mountain lee waves can be critical for aviation safety (Buck, 2000; Bolgiani et al., 2018; European Union Aviation Safety Agency, 2019; Gultepe et al., 2019). For this reason, aircrafts tend to incorporate anti-icing and/or de-icing systems in order to prevent and eliminate the accumulation of ice in the exposed frontal surfaces. Still, these devices are insufficient when aircraft icing events are extreme.

The National Transportation Safety Board reported that, between 2000 and 2011, meteorological conditions were involved in 37% of the accidents corresponding to commercial operations (Eick, 2014). According to the European Risk Classification Scheme for 2019 (European

Union Aviation Safety Agency, 2019), weather hazards were involved in the 15% of the accidents and serious incidents. Moreover, ice in flight and clear air turbulence (CAT) and mountain lee waves are ranked as the 3rd and 23rd, respectively, most hazardous type of events.

Mountain waves are a form of mechanical turbulence which develop downstream of mountains when a strong wind flows perpendicular to an orographic barrier and is forced to climb up the windward slopes. These waves can propagate vertically or horizontally (lee waves), when a slightly stable layer exists over the summit of the orographic barrier (Broutman et al., 2001; Lin, 2007). Violent downdrafts and updrafts produced by mountain lee waves, usually very close to the mountain barrier, are responsible for the turbulence in the lower levels of the leeward side. They often produce violent downdrafts on the immediate leeward side of the mountain barrier (Federal Aviation Administration, 2016). Also, these horizontal propagating waves generate rotors very close to the surface, as well as vertical windshear, being extremely

\* Corresponding author at: Department of Earth Physics and Astrophysics, Faculty of Physics, Complutense University of Madrid, 28040 Madrid, Spain.

E-mail address: [javidi04@ucm.es](mailto:javidi04@ucm.es) (J. Díaz-Fernández).

<https://doi.org/10.1016/j.atmosres.2021.105890>

Received 30 May 2021; Received in revised form 28 September 2021; Accepted 14 October 2021

Available online 22 October 2021

0169-8095/© 2021 The Authors.

Published by Elsevier B.V. This is an open access article under the CC BY-NC-ND license

(<http://creativecommons.org/licenses/by-nc-nd/4.0/>).

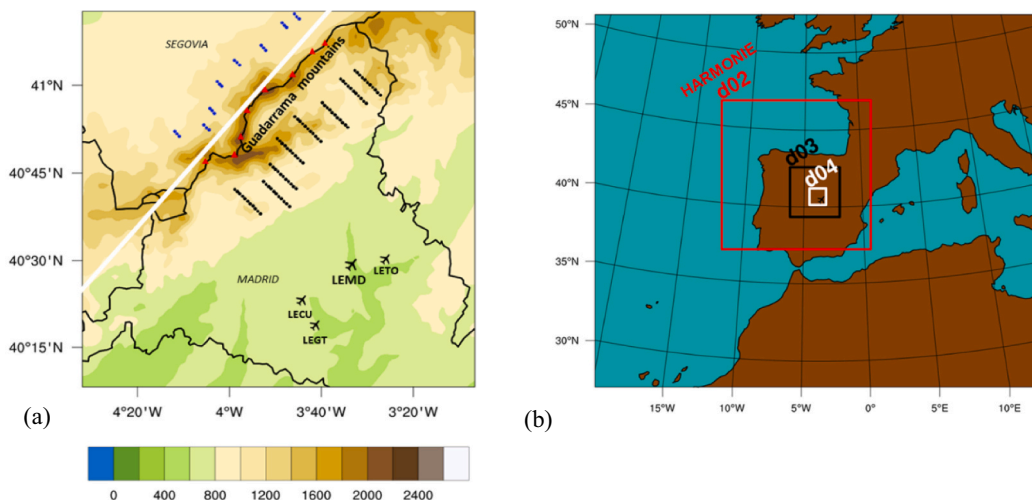


**Fig. 1.** (a) Orography of the research area (masl). Blue points (windward), red triangles (Guadarrama) and black dots (leeward) indicate the grid points where the mountain wave characterization is evaluated. The white line indicates the subdivision of the domain used in the BT analysis. Aircraft symbols correspond to airports' locations. (b) WRF and HARMONIE domain configuration. Outer boundary corresponds to outermost WRF domain (d01). LEMD location is marked with an aircraft symbol. (For interpretation of the references to colour in this figure legend, the reader is referred to the web version of this article.)

dangerous in terms of aviation safety (Klemp and Lilly, 1975; Doyle and Durran, 2002; Sharman et al., 2012; Udira et al., 2020). Vertical propagating waves are tied to a different form of turbulence due to the breaking of the waves. This occurs in the middle levels of the atmosphere, and they are dangerous for aviation as well (Kim and Chun, 2011; Lilly, 1978). Mountain waves have associated clouds also. Rotors produce a characteristic cloud when conditions are favourable. But most of the clouds generated by lee waves form in the updrafts, due to the adiabatic process of expansion which produces a temperature decrease and therefore a liquid water content (LWC) increase (Smith et al., 2002; Geresdi and Rasmussen, 2005; Bolgiani et al., 2018). The most distinctive are the lenticular clouds, which are presented as alternating bands of clouds, as they reside in the crests of the waves. These clouds are a common feature of the phenomenon, which makes it easily recognisable. However, they may be absent if the air is too dry. In the case a lee wave generates turbulence but no clouds, we can speak about a CAT event (Sharman et al., 2012; Evans, 2014).

Lenticular clouds can promote icing conditions if they are developed in an environment with temperatures below 0 °C. The accumulation of ice as the solidification of supercooled liquid hydrometeors on the surface of an aircraft, particularly in the front leading edges, is defined by Gent et al. (2000) as aircraft icing. This phenomenon affects the aviation safety due to the important changes in the aerodynamic generated by the ice accretion (Moran, 1989; Buck, 2000). Due to the lower efficiency of ice nucleation, aircraft icing is more likely to occur when the atmospheric temperatures range between −2 °C and −15 °C, as liquid water drops are predominant in environments up to −10 °C (Huffman and Norman, 1988; Rogers, 1993; Ledesma and Balariola, 2007). Both mountain lee waves and icing events are usual in the winter months, when the winds are stronger, the atmosphere is more stable and the melting level is lower (Wolff and Sharman, 2008). In addition, the Federal Aviation Administration (2016) reports that approximately 50% of the aircraft icing incidents occur at altitudes between 1500 and 4000 meters above sea level (masl), when atmospheric temperature ranges from −8 °C and −12 °C.

The accuracy of forecasting mountain lee waves and the phenomena associated using numerical weather prediction (NWP) models and remote sensing methods is not an easy process, mainly because of the lack of in-flight scientific observations directly taken inside the phenomena and the conjunction of several atmospheric factors (Weston et al., 2019). In fact, some authors sustain that icing studies are underdeveloped and require to be improved (Thompson et al., 2017).

The World Area Forecast Centres create turbulence and icing operational forecasts for aviation (Gill, 2014). Likewise, Significant Weather charts and Terminal Aerodrome Forecasts are a standard in the aviation industry (Storer et al., 2019). Nevertheless, turbulence and icing forecasting are far from perfect. Several research have tried to develop better tools for forecast icing conditions using NWP models. Firstly, algorithms based on temperature and air humidity (Schultz and Politovich, 1992; Thompson et al., 1997) and later implemented cloud microphysics schemes in operational NWP models to simulate the LWC (Olofsson et al., 2003; Gencer et al., 2010; Belo-Pereira, 2015). Sheridan and Vosper (2012) study the lee waves and downslope winds in Sierra Nevada (USA) using the Met Office Unified model and Udira et al. (2017) analysed a trapped lee-wave mountain event in the Pyrenees using the Weather Research and Forecasting model (WRF). On the other hand, Regmi et al. (2017) and Bolgiani et al. (2018) study aircraft icing reports associated to mountain lee waves events using WRF; and conclude that the main factor involved in the aircraft icing reports is the presence of supercooled liquid water. The WRF model was also used by Díaz-Fernández et al. (2020) to study several mountain lee waves episodes in the vicinity of Adolfo Suarez Madrid-Barajas airport (hereafter LEMD, as per the airport's International Civil Aviation Organization code; ICAO) analysing different physics parameterizations schemes. In connection with earlier results, Díaz-Fernández et al. (2021) characterized the atmospheric variables involved in 68 mountain wave episodes for ten years over a mountain range in central Spain, developing a warning method to forecast mountain lee waves events.

The same mountain wave episodes are evaluated using the HARMONIE-AROME (hereafter HARMONIE) and the WRF NWP models in the present paper. The brightness temperature (BT) simulated is compared in order to elucidate the performance of each NWP model to forecast the cloudiness associated to mountain lee waves. The characterization is performed using the percentiles from several atmospheric variables simulated involved in the mountain lee waves formation in the study area. Finally, a decision tree to warn mountain lee waves, lenticular clouds and icing events is carried out using the HARMONIE and comparing the results from both NWP models. This paper is performed within the framework of the SAFEFLIGHT research project whose objective is to develop and implement specific configurations of optimised high-resolution NWP models for forecasting mountain lee waves and icing events with the aim to improve the aviation safety in Spain.

It is worth commenting that the HARMONIE NWP model was developed and is used mainly as an operational model. However, the

interest of the research community in this model has been increasing thanks to the recent open data policy by European Centre for Medium-Range Weather Forecasts (ECMWF). Recently, several articles compared the HARMONIE and WRF models in different studies related to heavy precipitation and flooding (Toros et al., 2018; Varlas et al., 2019), fog (Román-Cascón et al., 2019) and subtropical cyclone (Quitián-Hernández et al., 2021). Nevertheless, to the authors' knowledge, this is the first time that this comparison is carried out for mountain lee waves studies in the Iberian Peninsula. Consequently, the existing literature related to mountain lee waves and HARMONIE model is limited.

The organization of this paper is as follows. The study area, the datasets and the description of the numerical models and the satellite data used are defined in Section 2. Section 3 explains the different methodologies used for the analysis of the BT, the characterization of the mountain lee waves and development of the decision tree and its validation. The main results derived from the methodology are exposed in Section 4; note that in order to facilitate the understanding of this paper, the results and discussion subsections are named after the corresponding methodology subsections. Finally, the major conclusions are summarized in Section 5.

## 2. Experimental design

### 2.1. Study area & datasets

The research area concerns the vicinity of the Guadarrama mountains (Fig. 1a). This mountain range is located in the centre of the Iberian Peninsula. It measures 80 km in length with a northeast to southwest orientation. Its highest peak is Peñalara reaching 2428 masl and located on the southern face. The selected area of study is characterized by the presence of LEMD airport, which is the main and busiest airport in Spain (6th in Europe as per passengers number), and other three smaller airports, all of them south-east of the Guadarrama mountain range. The orographic barrier has a great influence in the climatology and meteorology of the research area since the prevalent wind direction is from the North-West and mountain lee waves are usually formed on the leeward side. In order to characterize the mountain lee waves over the research area, 120 grid points are selected (Fig. 1a), following the same criteria used in previous studies over the same region (Díaz-Fernández et al., 2021). First, 8 of them are established over the summits of the range. Then, 3 are located windward (24 total) and 11 leeward points (88 total) are selected from the aforementioned, following the line of the prevalent wind direction and observing a buffer region at each side of the summits to avoid any distortion due to complex orography. The 11 consecutive grid points on the leeward face will cover at least one wavelength of the phenomenon.

The dataset for this study is the same that was used on Díaz-Fernández et al. (2021) to characterize the mountain lee waves with the WRF model. A data base of more than 180 mountain wave events between November to March is built from 2001 to 2019 using satellite images. This specific annual period is chosen considering the melting level is low and aircraft icing conditions are more likely to occur. From them, 13 events (2017–2019) are selected to validate simulated BT versus observational satellite data, the 68 clearer events (2001–2010) are used to establish the characterization of mountain wave formation and finally 6 episodes (2017–2020) are randomly chosen to validate the decision tree (see Appendix A). These days are simulated for the present article using the HARMONIE model.

### 2.2. Numerical weather prediction models

The events abovementioned have been simulated using two NWP models in order to compare both. It is important to remark that both models are different from the very basic features, and thus, it is not sensible trying to perfectly match the configurations or the analysis of

the results. Nevertheless, they are here run considering their features in a way as similar as possible. Earlier comparisons have been successfully performed for other meteorological events (Quitián-Hernández et al., 2021; Román-Cascón et al., 2019). A brief description of each is provided.

#### 2.2.1. WRF

The WRF NWP model version 4.0.3 is used in this study (Skamarock and Klemp, 2008). Different initial conditions are used for each subsection, to optimise the results using similar products. For the BT analysis a high resolution was required, thus initial and boundary conditions are extracted from the National Centers for Environmental Prediction (NCEP) Global Forecast System (GFS) analysis, with a horizontal spatial resolution of  $0.25^\circ$  and a temporal resolution of 3 h (NCEP, 2015). However, this product does not cover the whole 2001–2010 period, so for the characterization, NCEP Climate Forecast System Reanalysis (CFSR) data are taken, with a horizontal spatial resolution of  $0.5^\circ$  and a temporal resolution of 6 h (Saha et al., 2010). Finally, for the validation of the decision tree, the initial conditions are chosen from the NCEP GFS 24 to 48-h forecast, at a  $0.25^\circ$  horizontal spatial resolution and 3 h temporal resolution (NCEP, 2015), to match the most similar conditions available to a real operational tool.

Each episode is simulated in periods of 24 h, considering the first 6 h as spin-up time. The simulation is run with four nested domains using  $121 \times 121$  grid points in north-south and east-west directions and 60 sigma vertical levels for each domain. Horizontal resolution of the domains was 27, 9, 3 and 1 km, respectively. In Fig. 1b, the outer domain (d01) covers southwestern Europe and North Africa. Domain d02 approximately includes the Iberian Peninsula. Domains d03 and d04 are centred over the Guadarrama mountain range and covering the main area of study.

Regarding the physical parametrizations used in the WRF simulations, the Dudhia shortwave scheme (Dudhia, 1989) and RRTM long-wave scheme (Mlawer et al., 1997) are used for radiation; the Unified Noah land-surface model (Tewari et al., 2004); revised MM5 (Jiménez et al., 2012) as the surface layer scheme and the Yonsei University (YSU; Hong et al., 2006) as the Planetary Boundary Layer (PBL) scheme are chosen. Finally, the Thompson parametrization (Thompson et al., 2008) is used for microphysics. This configuration was validated and revealed as the optimum parameterization schemes to simulate lenticular clouds associated to mountain lee waves in the same study area by Díaz-Fernández et al. (2020) and was later employed for the mountain wave characterization (Díaz-Fernández et al., 2021).

#### 2.2.2. HARMONIE-AROME

The HARMONIE model (version 40 h1.1.1) is a non-hydrostatic spectral, semi-implicit and semi-lagrangian model. This model is developed and maintained by the collaboration between the ALADIN (Aire Limitée Adaptation Dynamique Développement International) and HIRLAM (High-Resolution Limited Area Model) consortium (Bengtsson et al., 2017). Initial and boundary conditions are taken from the ERA5 Integrated Forecast System (IFS) from European Centre for Medium-Range Weather Forecasts (ECMWF) global model with a 31 km horizontal resolution and 1 h temporal resolution (Hersbach et al., 2020).

Here, HARMONIE is used in a non-standard setup, optimised for research purposes instead of operational ones, taking into account a smaller domain than the usually used in operational mode. The HARMONIE simulations run on a single domain covering the same d02 WRF area (Fig. 1b), as this model does not require nesting to downscale the resolution from the initial conditions to the grid size. However, only the area corresponding to d04 WRF domain is evaluated to preserve the consistency between both models. The horizontal resolution is 1 km, and the model has 65 hybrid sigma pressure levels. Regarding the physical parametrizations, the default physics options defined by Bengtsson et al. (2017) have been used. It is worth remarking that this is an operational model, fine-tuned to serve as a general-purpose tool, not dedicated to the

study of a single phenomenon or area. Thus, there are not many configuring options regarding the physics suite, as the NWP model is already and continuously optimised for its objective by the development team. This is also the reason behind the lack of scientific literature regarding this model, but at the same time a great incentive for research.

Note that different initial conditions have been used for both models. The reason for this difference is to use the more accurately initial conditions for each model, NCEP GFS have been run with WRF and ERA5 with HARMONIE. Moreover, HARMONIE does not allow to run with NCEP GFS. Bolgiani et al. (2020) run the WRF with ERA5 and NCEP GFS as initial conditions and compared both, obtaining very similar results in a microburst study. Other comparative study (Zhang et al., 2020) obtained better wind speeds correlations in WRF simulations with NCEP GFS than ERA5.

### 2.3. Satellites

Mountain wave events were selected using imagery from the Meteosat satellite family. These geostationary satellites are managed by the European Organization for the Exploitation of Meteorological Satellites (EUMETSAT). The horizontal resolution is 3 km at nadir for the 10.8  $\mu\text{m}$  infrared channel, 2.5 km at nadir for the 0.6  $\mu\text{m}$  visible channel and 1 km for the high-resolution visible channel (Schmetz et al., 2002) and the temporal resolution is 15 min.

In the mountain wave characterization process, we select an event using the 0.6  $\mu\text{m}$  visible channel of the Meteosat Visible and Infrared Imager (MVIRI) up to December 2006, and the high-resolution visible channel of the Meteosat Second Generation Spinning Enhanced Visible and Infra-Red Imager (MSG-SEVIRI) from January 2007 on. The images are evaluated in search of the associated lenticular clouds, as these are a clear indication for the existence of mountain lee waves. For the BT analysis, the 10.8  $\mu\text{m}$  infrared channel of the MSG-SEVIRI is used to validate the HARMONIE and WRF simulations. Finally, the Red-Green-Blue (RGB) satellite image composition (1.6  $\mu\text{m}$  in the red beam, 0.8  $\mu\text{m}$  in the green beam and 0.6  $\mu\text{m}$  in the blue beam) is used in order to detect icing clouds tops in the decision tree validation, as per Lensky and Rosenfeld (2008) procedure.

### 3. Methodology

The data base of mountain wave episodes is created using the previously described satellite images for the diurnal period (08:00 to 17:00 UTC), and observing the following conditions already described by Díaz-Fernández et al. (2021):

- Lenticular clouds present south-east of the Guadarrama mountain range.
- A minimum of 3 alternating cloud bands parallel to the mountains, with wavelengths and transversal lengths greater than 15 km.
- The BT of the lenticular clouds ranging between 260 and 275 K.

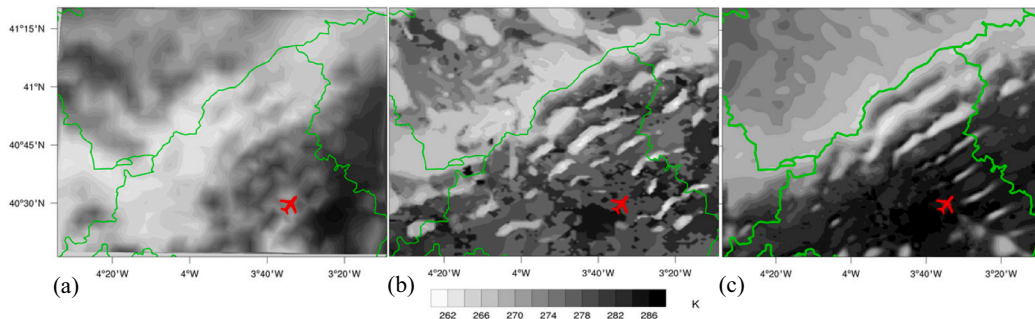


**Fig. 2.** BT images on 26 November 2018 at 13:00 UTC. (a) MSG-SEVIRI image in the 10.8  $\mu\text{m}$  band. (b) WRF pseudo satellite image. (c) HARMONIE pseudo satellite image. Aircraft symbol corresponds to LEMD location.

Considering these requirements, the 68 days described in the database are produced, making a total of 680 hourly results when the daily period and time resolution are taken into account.

#### 3.1. Brightness temperature analysis

Following Díaz-Fernández et al. (2020), the BT is used to compare observed and simulated lenticular clouds. The 10.8  $\mu\text{m}$  infrared channel from MSG-SEVIRI is used as observational data. This long-wave infrared channel is the most suitable one to detect the cloud top and the surface temperature (Chevallier and Kelly, 2002; Otkin et al., 2009; Bormann et al., 2014). To avoid any distortion from orographic clouds, the research area is cropped along the Guadarrama mountain range, as depicted in Fig. 1a (white line). In this way, the BT analysis is carried out only for the south-eastern part of the Guadarrama mountains (leeward side), where the lenticular clouds are formed.

The BT frequency distribution is then obtained in the leeward research area for the WRF, HARMONIE and MSG-SEVIRI data to determine the cloud tops and altitude distribution (Bormann et al., 2014; Quitián-Hernández et al., 2021). Lastly, temporal and spatial skill score averages for Bias, Root-Mean-Square Error (RMSE), Mean Absolute Error (MAE), Standard Deviation (SD) and Linear product-moment correlation coefficient of Pearson (R) are calculated to summarize the information into a single value (Díaz-Fernández et al., 2020).

#### 3.2. Mountain lee waves characterization

Wind direction and speed, static stability (ST), LWC and temperature are obtained using the HARMONIE model in each of the 120 grid points evaluated (Fig. 1a) for the 680 time steps. This way, we can easily compare with the earlier WRF results obtained with the same procedure by Díaz-Fernández et al. (2021). As the simulated variables reveal very similar results for every point of each group, the values are averaged in three single outcomes: windward, Guadarrama and leeward.

The formulation used to compute the ST is (Bluestein, 1992; Young, 2003):

$$ST = \frac{-\left(\frac{T}{\theta}\right) * d(\theta)}{dp} \quad (1)$$

where T the temperature,  $\theta$  is the potential temperature and p is the pressure.

Once the averaged results in every area are derived, HARMONIE and WRF probability density functions for lenticular clouds and non-clouds events are assessed and the percentiles (P) 10, 25, 50, 75 and 90 are computed for each of the selected variables. The WRF atmospheric variables above mentioned were chosen at 2800 masl, because such an altitude presents the highest values of LWC initially detected (Bolgiani et al., 2018; Díaz-Fernández et al., 2020). For HARMONIE, the data are



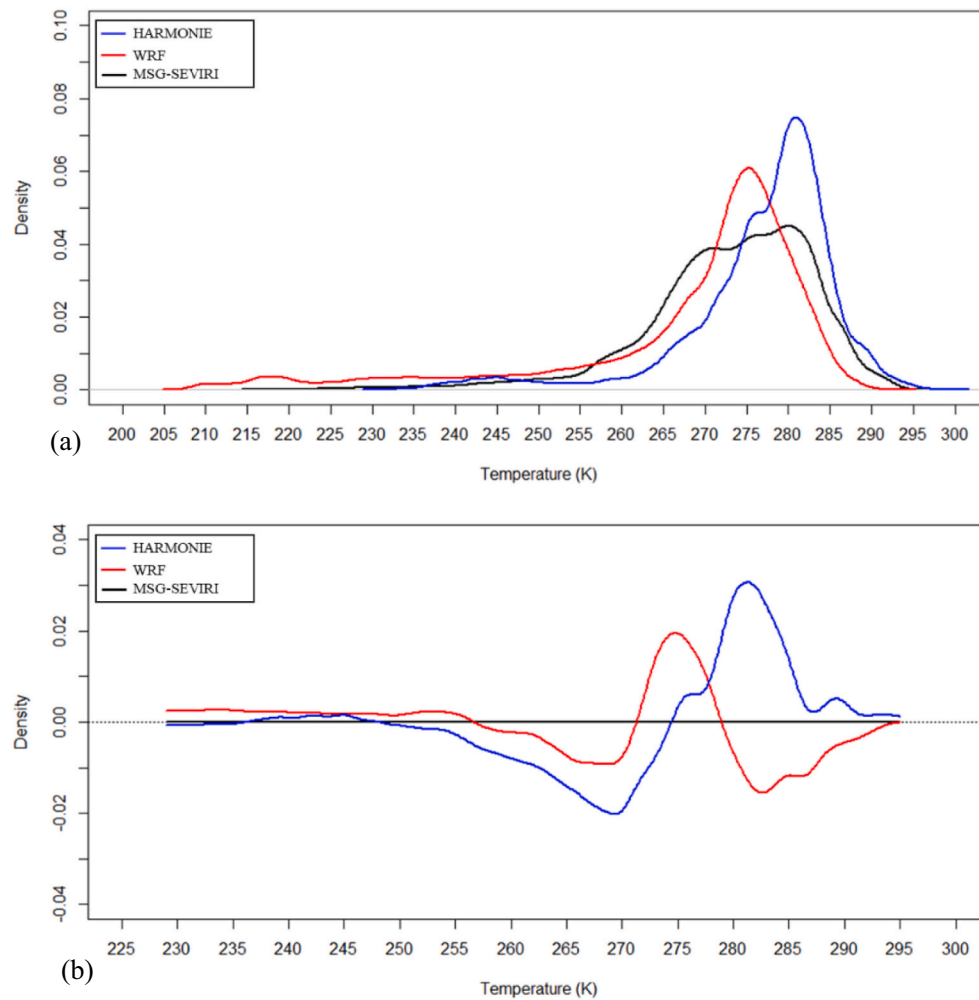


Fig. 3. WRF, HARMONIE and MSG-SEVIRI outcomes of: (a) BT probability density functions; (b) BT error for 13 mountain lee waves selected events.

computed at 720 hPa since this isobaric level corresponds to an altitude of 2800 masl, according to the International Standard Atmosphere.

### 3.3. Decision tree and validation

With the HARMONIE model mountain wave characterization results, a warning decision tree is created, similarly as it was previously done using WRF output (Díaz-Fernández et al., 2021). This warning algorithm is created considering several percentile values from the HARMONIE simulations, which are as follows: In a first step, mountain lee waves are warned using P10 and P90 for wind direction, wind speed and ST. If the previous is positive, i.e., mountain wave warning is achieved, a lenticular clouds warning can be derived by incorporating the LWC P10. Finally, if the previous is also active, P10 for temperature is considered for an icing conditions warning.

As in Díaz-Fernández et al. (2021), the three warnings are validated using a contingency table for dichotomous verification of HARMONIE forecasts (at least 24 h before the event) for six random days (approximately 10% of the dataset of mountain wave events). This verification is carried out during the diurnal period only (08:00–17:00 UTC), to keep consistency with the characterization. Subsequently, the False Alarm Ratio (FAR), Probability Of Detection (POD), frequency BIAS, and Percent Correct (PC) are computed to check the warning skills of the decision tree (López et al., 2007; Kunz, 2007; Aznar et al., 2010; Díaz-Fernández et al., 2021).

## 4. Results and discussion

To start off, the mountain wave episode of 26th November 2018 with north-west wind direction is presented as an example and analysed taking into account the MSG-SEVIRI images. Fig. 2 shows the ability of the WRF and HARMONIE models to reproduce lenticular clouds bands associated to mountain lee waves as it would be seen in the pseudo satellite images. Fig. 2a corresponds to the satellite observation, which presents the poorest quality, as the spatial resolution in the research area is 5 km approximately (Combal and Noel, 2009). Notwithstanding, alternate lenticular clouds are suggested north of LEMD airport with BTs between 260 and 266 K. Comparing the WRF (Fig. 2b) and HARMONIE (Fig. 2c) pseudo satellite images, at least 6 alternate lenticular cloud bands can be observed on the leeward side of the Guadarrama mountains. The BTs of the lenticular clouds in both pseudo satellite images are very similar (lower than 266 K). However, the HARMONIE BTs for the cloudless areas are greater than the corresponding WRF temperatures. Similar results have been observed by Quitián-Hernández et al. (2021), suggesting a warm BIAS of the HARMONIE model for surface temperature. Another noteworthy difference is the lenticular clouds simulation for each model. While HARMONIE produces a smooth and continuous cloud, WRF simulates broken clouds, mostly noticeable in the first three bands. Also, as the wave moves away from the mountain, HARMONIE simulates relatively thin cloud bands, while WRF produces more abundant, thick clouds.

With this event in mind, we can now proceed to evaluate the results.

**Table 1**

WRF and HARMONIE average spatial skill scores of BT (K) for the 13 mountain lee waves selected events. Best scores are highlighted in bold.

	MSG-SEVIRI	WRF	HARMONIE
Average	273.10	268.16	<b>276.79</b>
SD	10.04	15.73	<b>9.36</b>
RMSE	–	15.72	<b>9.94</b>
MAE	–	10.41	<b>7.18</b>
BIAS	–	–4.94	<b>3.69</b>
R	–	0.50	<b>0.55</b>

First, the WRF and HARMONIE BT frequency distributions are analysed and compared. Subsequently, the probability density functions of the atmospheric variables for both models are presented to characterize the mountain lee waves. Finally, a warning decision tree is developed and validated for the HARMONIE model, and then compared with the WRF validation obtained by Díaz-Fernández et al. (2021).

#### 4.1. Brightness temperature analysis

The BT analysis is performed by using the simulations and observations for 13 days. The probability density functions (Fig. 3a) are shown for both models and the observational data. Also, the BT error of each model against the satellite observation is presented (Fig. 3b). The results of the probability density function show that WRF simulates lower BT (higher clouds) than observed, about  $-10$  K, while the HARMONIE distribution does not reach the lowest temperatures observed approximately by 15 K. Focusing on the other tail of the distribution, WRF and MSG-SEVIRI curves are close to each other for the greatest temperature values (surface terrain), whereas HARMONIE overestimates these temperatures approximately 5 K. This displacement of the simulated curves over the BT axis suggests a cold BIAS for the WRF and a warm BIAS for the HARMONIE model. Quitián-Hernández et al. (2021) compared WRF and HARMONIE BT in a study of subtropical cyclones with very similar results to the ones here presented, since HARMONIE overestimated the surface BT and WRF underestimated them, like the prevailing research.

In the range of temperature values where lenticular clouds usually develop, which is between 260 and 275 K, the models behave differently. While HARMONIE underestimates the density in all the range, clearly visible in the error results (Fig. 3b), WRF underestimates below 270 K, but overestimates above the latter value. This is consistent with the previous results shown in Fig. 2, where it was clear that HARMONIE tends to simulate a lower number of clouds, albeit these are only valid

for a single event. Finally, both models and the observations present asymmetric distributions with mode values of 280 K for the MSG-SEVIRI, and 275 K and 281 K for WRF and HARMONIE, respectively. Moreover, it is noteworthy the difference of 6 K between the WRF and HARMONIE mode values, pointed also in Quitián-Hernández et al. (2021). Similar probability density function shapes for the WRF model were obtained by Otkin et al. (2009) and Bormann et al. (2014). Moreover, the results here presented are in line with those of Jankov et al. (2011) and Shi et al. (2018), who simulated by WRF greater values of BT than the satellite observations in cloudiness related studies.

One possible explanation for the BT underestimation simulated by WRF can be found in the Bormann et al. (2014) studies that related simulated BT with observed one from MSG-SEVIRI. According to these authors, the surface emissivity and the diurnal cycle of surface temperature in clear-sky conditions are not well modelled, which is reflected in the satellite pseudo-images simulated by WRF in the  $10.8 \mu\text{m}$  channel (the same used here).

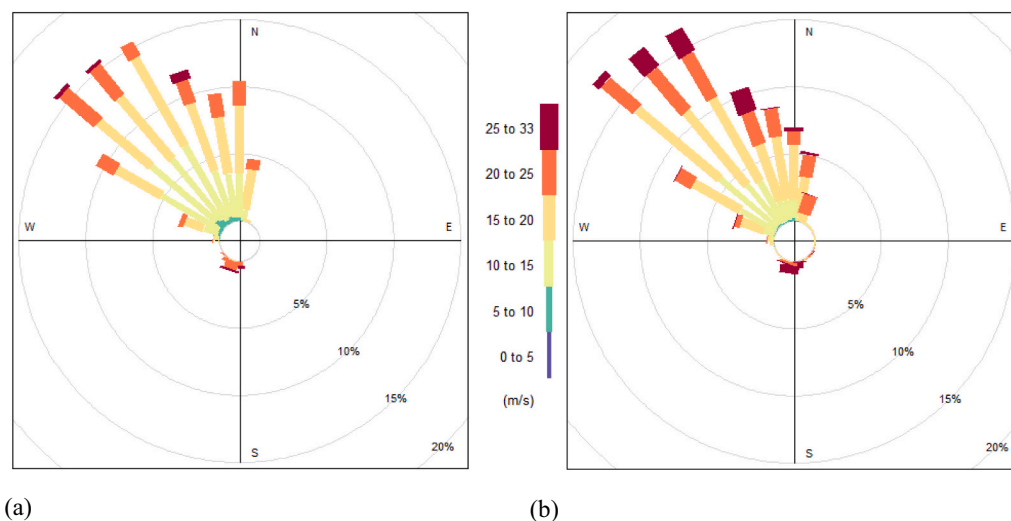
The BT error (Fig. 3b) shows in a clearer way the underestimations and overestimations of each model against the observations. Apart from the range of lenticular clouds BTs, already commented, the error results show that the WRF model tends to overestimate the amount of high clouds (lower BTs). Regarding the surface temperature (above 275 K), the HARMONIE model notably overestimates them while WRF tends to underestimate, which is again consistent with the BIAS described before.

Table 1 shows the skill scores averaged for the domain of study computed for the observations and NWP models used. Comparing the BT average and SD, HARMONIE shows the closest value for both skill scores. Regarding error scores (RMSE and MAE), there are considerable differences since HARMONIE obtains lower errors than WRF. The performance of BIAS score for both models is opposite, as expected from previous results. HARMONIE overestimates (3.69) while WRF underestimates ( $-4.94$ ) the BT. Finally, the R results are quite similar with approximate values of 0.50, statistically significant at 99% level.

Considering the overall results from the BT analysis, HARMONIE reveals as the most accurate model to simulate the BT. However, in the lenticular clouds range (260–275 K) the BT curve simulated by WRF is closer to the satellite observations than the one corresponding to HARMONIE.

#### 4.2. Mountain lee waves characterization

As described in the methodology (Section 3.2) and following the same procedure as Díaz-Fernández et al. (2021), simulated atmospheric



**Fig. 4.** Simulated average wind direction rose for the total lenticular clouds events on the windward side for: (a) HARMONIE. (b) WRF. (For interpretation of the references to colour in this figure legend, the reader is referred to the web version of this article.)

**Table 2**

HARMONIE and WRF lenticular clouds percentile values for the evaluated atmospheric variables. Values in bold show the thresholds used in the decision trees.

		WRF	HARMONIE
Wind Direction (degrees)	P10	<b>295</b>	<b>294</b>
	P25	308	310
	P50	326	328
	P75	346	346
	P90	<b>003</b>	<b>359</b>
Wind Speed (m/s)	P10	<b>12.7</b>	<b>11.7</b>
	P25	15.2	13.6
	P50	17.9	16.0
	P75	20.7	18.9
	P90	24.2	21.7
ST (K/Pa)	P10	<b>−0.0600</b>	<b>0.0002</b>
	P25	−0.0200	0.0004
	P50	0.0000	0.0007
	P75	0.0200	0.0011
	P90	<b>0.0500</b>	<b>0.0014</b>
LWC (g/kg)	P10	<b>0.00</b>	<b>0.00</b>
	P25	0.02	0.05
	P50	0.34	0.28
	P75	0.76	0.47
	P90	1.06	0.72
Temperature (°C)	P10	<b>−14.7</b>	<b>−13.6</b>
	P25	−10.8	−10.6
	P50	−8.2	−7.9
	P75	−4.5	−5.3
	P90	−2.0	−2.4

variables for 68 selected events are evaluated over 120 grid points (Fig. 1a) to create a characterization of the mountain lee waves in the area of study. The results are subdivided in two categories, with the presence of lenticular clouds and without it. These are then compared between the models HARMONIE and WRF.

The atmospheric variables considered (wind direction, wind speed, atmospheric stability, liquid water content and temperature) are not equally relevant in every step of the process, thus, a preferential location is evaluated for each one. Wind variables (speed and direction) are assessed on the windward side at 2800 masl before the wind is forced upslope. The prevalent wind direction for both models during lenticular clouds is north-west (Fig. 4). Regarding the percentiles (Table 2), the differences between both models are negligible, as the largest one corresponds to the P90 value (359° and 003° for HARMONIE and WRF, respectively). This prevailing wind direction matches with the necessary

condition (wind direction perpendicular to the orographic barrier) to develop lenticular clouds in the leeward side.

Fig. 5 shows the average wind speed probability density function for both models. It can be seen that the wind speed in lenticular clouds events is greater than in non-cloud events (more clear in WRF). However, it is also noteworthy that the wind speed is greater for WRF than for HARMONIE (Table 2). The percentiles show that the difference increases the wind speed strengths. Thus, the P10 difference between WRF and HARMONIE is 1 m/s while in the P90 is 2.5 m/s. The percentiles for lenticular clouds events (Table 2) indicate that 80% of the hours, the wind speed simulated by HARMONIE ranges from 11.7 to 21.7 m/s and from 12.7 to 24.2 m/s for WRF. These results are consistent with an observed value of wind speed (21.1 m/s) registered during a lenticular clouds event reported in the same area and studied by Bolgiani et al. (2018). Highlighting that this value fits within 80% of wind speed values simulated for both models in the present mountain wave characterization.

The ST is evaluated over the eight selected grid points over the Guadarrama mountains to avoid the influence of a possible orographic dipole formation in the windward and leeward sides at 2800 masl (Fernández-González et al., 2014; Díaz-Fernández et al., 2020). A stable layer over the Guadarrama mountains promotes the mountain wave formation. However, neutral stability conditions ( $ST \approx 0$  K/Pa) attenuate the horizontal wave propagation (Koch and O'Handley, 1997; Fernández-González et al., 2014, 2019; Díaz-Fernández et al., 2020).

The ST probability density functions for lenticular clouds events and non-clouds events for HARMONIE and WRF are depicted (Fig. 6). This atmospheric variable shows the greatest differences between both models. HARMONIE simulates all the ST values around neutral and slightly positive stability with probability density values much greater than those obtained for WRF. 80% of the WRF ST values correspond to instability and weak stability (from  $-0.06$  to  $0.05$  K/Pa), being the P50 value the neutral stability (Table 2). Not many differences between lenticular cloud events and non-clouds ones are observed for both NWP models. These ST values simulated by WRF agree with previous mountain lee waves studies (Fernández-González et al., 2014, 2019; Díaz-Fernández et al., 2020), although the HARMONIE percentiles (Table 2) are more consistent with the slight positive stability conditions required for mountain lee waves generation.

On the other hand, the difference of roughly two orders of magnitude in the percentile values for both models need to be addressed. These unexpected results generated further research to find the origin of such differences. In order to try to clarify this issue, WRF and HARMONIE

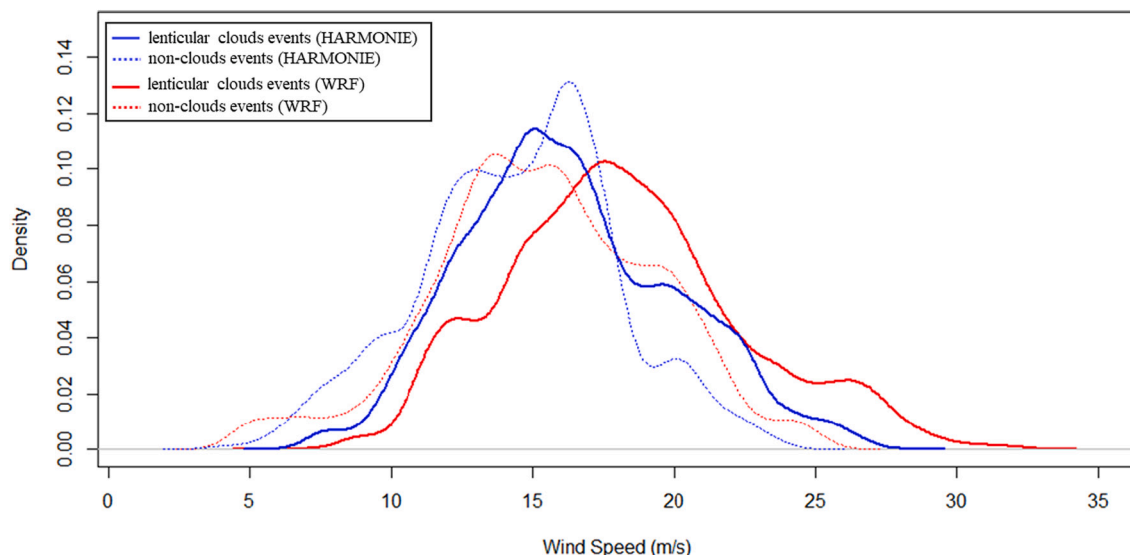
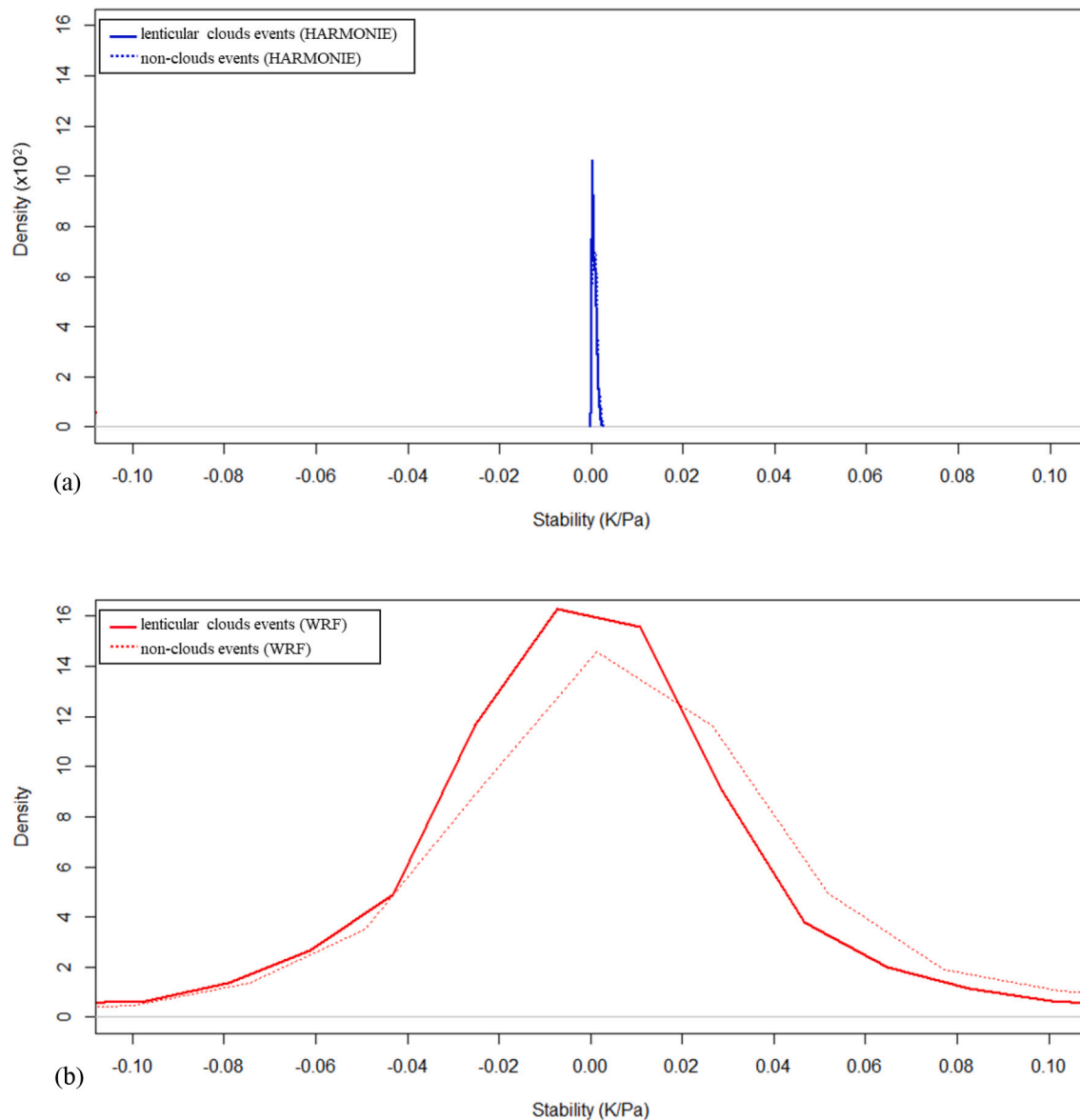


Fig. 5. Average wind speed probability density function on the windward side for HARMONIE and WRF models for lenticular clouds and non-clouds events.



**Fig. 6.** Average ST probability density functions over the Guadarrama mountains for: (a) HARMONIE ( $\times 10^2$ ) and (b) WRF for lenticular clouds and non-clouds events. Note that the shape for ST HARMONIE probability density function (a) is almost equal in lenticular clouds events and non-clouds events.

vertical profiles for pressure, dew point and temperature are compared with LEMD soundings (the only sounding available in the study area) for the validation period. The results show high R values for both models, more than 0.96 for temperature and dew point. These R results agree with the mountain lee waves study over Guadarrama mountains by Navia-Osorio (2012). For the wind speed R is 0.84 (WRF) and 0.88 (HARMONIE). In the ST there are more differences, 0.70 for WRF and 0.73 for HARMONIE. Relative to BIAS, the wind speed is underestimated by HARMONIE and the ST is slightly overestimated by WRF. Both models show a slightly overestimation in the temperature vertical profile. However, between surface and 700 hPa, the temperature vertical profiles depict that the WRF's temperature difference is about 3 K greater than HARMONIE's temperatures. This temperature variation would explain the WRF ST differences to at least an order of magnitude greater than HARMONIE. The higher RMSE results correspond to dew point (between 4.5 and 5.5 °C) and wind speed (between 3 and 4 m/s). Due to the obtained high correlation values and the good remaining skill scores results for the sounding simulated by both models in LEMD, it could be considered that the vertical profiles for HARMONIE and WRF agree with the sounding observations in the windward area of the

domain. Thus, as an example simulated soundings of a mountain lee wave event for WRF and HARMONIE are depicted in Fig. 7 for the windward side. It can be noted the similarities between temperature and dew point for both models, being in the surface the WRF temperature slightly higher than HARMONIE. Relative to wind speed and direction both NWP models match.

Moreover, it was observed the skill of WRF to simulate thermal inversions in contrast to the HARMONIE model, which would explain why the ST range for the WRF model runs from negative values (instability) to positive values (stability) and in HARMONIE it ranges between the neutrality to stability (positive ST values). These results are in concordance with Qutián-Hernández et al. (2021) comparison of 2-m temperatures and vertical profiles in WRF and HARMONIE, obtaining greater temperatures for the former in the lower vertical levels.

The maximum LWC and minimum temperature are evaluated in the leeward grid points, where the mountain wave may be formed, producing the associated cloud. As expected, maximum LWC probability density function results (Fig. 8) show lower levels for non-clouds events. Comparing both models in lenticular clouds events, HARMONIE tends to simulate lower LWC values with a marked decrease from 0.4 g/kg. On



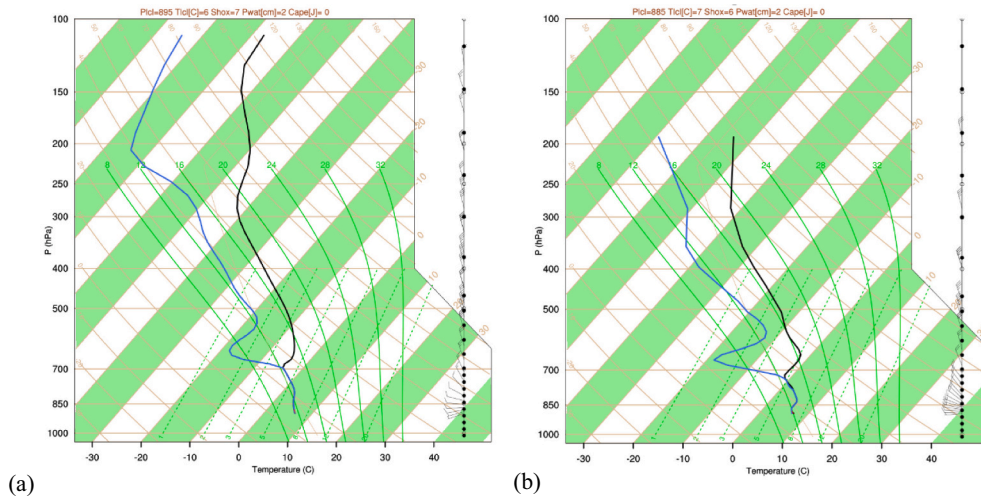


Fig. 7. Simulated sounding for HARMONIE (a) and WRF (b) in an example mountain lee waves event on the windward side.

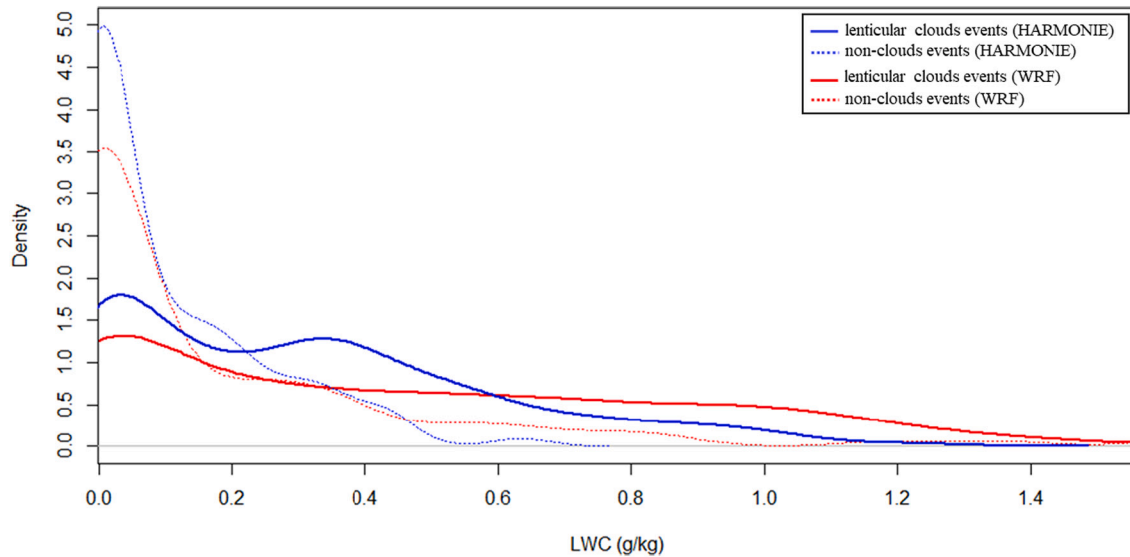


Fig. 8. Maximum LWC probability density function on the leeward side for HARMONIE and WRF models for lenticular clouds and non-clouds events.

the other hand, WRF curve is smoother, presenting similar densities from 0.2 to 1.0 g/kg, thus generating more situations with high LWC values. This is also demonstrated in the LWC percentiles (Table 2).

Tafferner et al. (2003) used numerical simulations to establish several categories of aircraft icing. The LWC limit value whereby icing conditions do not affect aviation safety is 0.1 g/kg for one hour. A light aircraft icing is produced with LWC values between 0.1 and 0.5 g/kg. LWC values 0.5 to 1 g/kg generate moderate aircraft icing, while values greater than 1 g/kg could produce a severe aircraft icing. Beyond the consideration of the LWC for the formation of lenticular clouds, the LWC value of 0.1 g/kg, from which produces icing conditions, is reached or exceeded by both models 69% of the times.

Once lenticular clouds are generated, the presence of temperatures below 0 °C is a necessary requirement to develop supercooled liquid water and therefore icing conditions (Raubert and Tokay, 1991; Buck, 2000). Thus, temperature is also evaluated on the leeward grid points. The minimum temperature probability density function for lenticular clouds events (Fig. 9) is similar to the non-clouds events for both WRF and HARMONIE. However, the WRF temperature range is greater than the HARMONIE range, as it can be seen also in the percentile's values (Table 2). In the process of supercooled liquid water drops formation

(icing conditions), the ice nucleation processes are less efficient than condensation for temperatures below −15 °C (Huffman and Norman, 1988; Wang, 2010; Fernández-González et al., 2014). For that reason, it should be noted that 90% of the minimum temperatures are found between 0 and −15 °C in WRF lenticular clouds events and 93% in HARMONIE ones. This implies that most of the times that lenticular clouds are simulated by any of the models, icing conditions exist, which is consistent with the annual period of study.

#### 4.3. Decision tree and validation

Following the methodology described in Section 3.3, the HARMONIE decision tree is developed to forecast mountain lee waves, lenticular clouds and icing warnings according to the percentiles highlighted in bold in Table 2. A similar algorithm was developed for the WRF results in Díaz-Fernández et al. (2021) using the same methodology. A schematic explanation is now sketched out, but an interested reader can find the details in Díaz-Fernández et al. (2021):

The mountain wave formation process influences the hierarchy of the atmospheric variables in the decision tree. Thus, the steps to build the algorithm are:

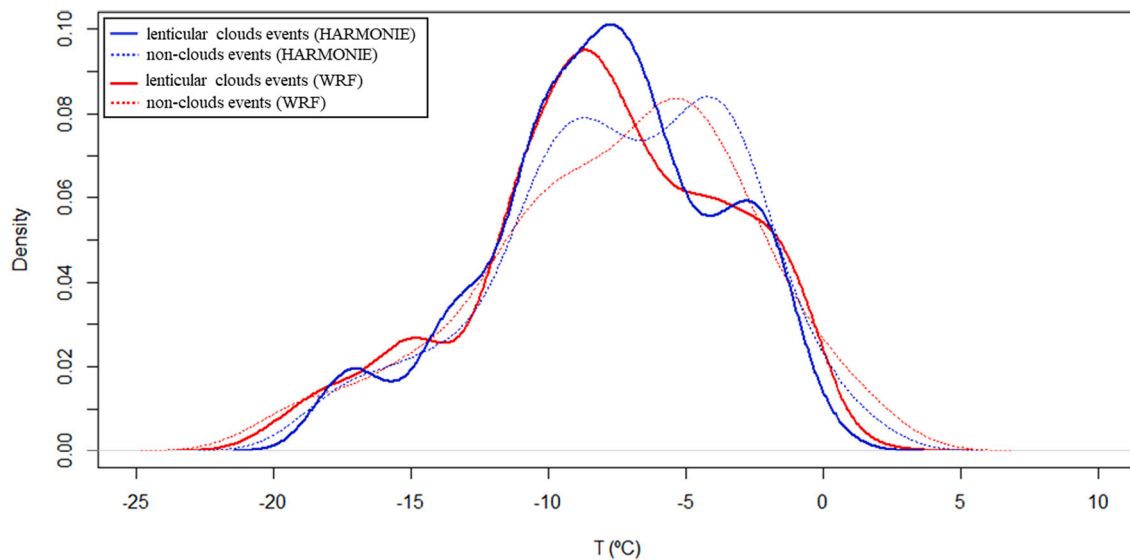


Fig. 9. Minimum temperature probability density functions on the leeward side for HARMONIE and WRF models for lenticular clouds and non-clouds events.

- First, windward wind direction is evaluated. The P10-P90 interval is considered as requirement.
- Then, windward wind speed is assessed. A threshold is established in P10 as requisite to establish a warning.
- If the two previous conditions are met, ST thresholds over Guadarrama are evaluated at the third step. Between P10 to P90 values is considered as requisite to promote mountain wave formation and therefore a mountain wave warning.
- If a mountain wave warning is issued, the maximum LWC is then considered in the leeward side. If  $LWC > 0 \text{ g/kg}$  (P10), lenticular clouds warning is also issued.
- Only if a lenticular clouds warning has been reached, the minimum temperature range is considered in the fifth step. If leeward minimum temperature ranges between P10 and  $0^\circ\text{C}$ , an icing warning is also produced.

The result for the HARMONIE decision tree is depicted in Fig. 10. Particularly for this model, the first condition required the wind direction to be between  $294^\circ$  and  $359^\circ$ . This interval corresponds to 80% of the range observed in the mountain lee waves characterization. Wind speed in the windward side must then be equal or higher than  $11.7 \text{ m/s}$ , which corresponds to 90% of the wind speed values in the characterization. Third, the ST over Guadarrama should be between 0.0002 and  $0.0014 \text{ K/Pa}$  (P10 and P90, respectively). If these three conditions are not met, a mountain wave warning would not be possible.

If the mountain wave warning is active, to provide a lenticular clouds warning the LWC in the leeward side must be greater than  $0.00 \text{ g/kg}$  (P10). Finally, an icing warning is established if the temperature range lies between  $0.0^\circ\text{C}$  and  $-13.6^\circ\text{C}$  in the leeward side (entailing that the mountain wave and lenticular clouds warnings are also active).

To validate the decision tree warnings six episodes are simulated using HARMONIE forecasts at least 24 h before the event. The verification process follows the same procedure used in Díaz-Fernández et al. (2021) to validate the corresponding WRF algorithm. The skill scores described in the methodology (Section 3.3) are calculated for the HARMONIE decision tree warnings and the results for both models are compared in Table 3. As the mountain lee waves without lenticular clouds cannot be validated using satellite data, the satellite observations of cloud bands are used to validate both mountain lee waves and the associated lenticular clouds. The icing verification is done using the RGB composition from MSG-SEVIRI to detect ice clouds.

Attending the mountain lee waves warning for both models (Table 3), there are differences in the BIAS score, since WRF

overestimates but HARMONIE underestimates them. In the remaining skill scores, WRF obtains a better POD and similar FAR than HARMONIE, while PC are similar for both models. Regarding the warning for lenticular clouds, FAR and PC values are essentially the same for both NWP. However, POD and BIAS results for WRF are better than those obtained by HARMONIE. The skill scores evaluated for icing warning globally reveal HARMONIE as the most appropriate forecasting tool, performing better than WRF in FAR, POD and PC, with only a slight underestimation shown in the BIAS against the perfect score produced by the WRF model. However, it should be noted that lenticular clouds and icing conditions warning results must be considered only under the scope of the previous warning results. As an icing warning will only be issued when a lenticular clouds warning is active, and this will only be issued when a mountain wave warning is active, the skill score results are dependent on those for the previous phase.

Despite the POD skill scores may seem low (Table 3), it is worth noting that according to the World Meteorological Organization (2005), a POD value higher than 0.5 should be considered as an event with high probability of occurrence and it is recommended to forecast it as an assertive event in the meteorological reports. Therefore, all warning for both models may be implemented in operational forecasts, as every POD result is 0.59 or above. Concerning the BIAS scores for WRF, Carvalho et al. (2014) proved that the surface wind speed in wind farms in Portugal is usually overestimated by the WRF model. Nevertheless, Rasheed et al. (2014) demonstrated that the HARMONIE model under-predicted the wind magnitude over complex terrain in Norwegian wind farms. These results are in line with the overestimation (WRF) and underestimation (HARMONIE) found in the mountain lee waves warnings (Table 3) and in the wind speed characterization (Fig. 5).

Previous studies demonstrated that the WRF model is able to capture mountain lee waves with no presence of lenticular clouds (Fernández-González et al., 2014; Bolgiani et al., 2018; Díaz-Fernández et al., 2020). This is a key issue because, as mentioned above, the mountain lee waves warning is verified only against lenticular clouds observations in the current study. This would render at least a part of that overestimation as the correct detection of mountain lee waves which could not be observed due to the absence of lenticular clouds. In contrast, the underestimation shown for the lenticular clouds warning can be partially explained by the fact that both NWP models are inclined to underestimate the LWC (Naud et al., 2014; Fernández-González et al., 2014; Huang et al., 2015; Merino et al., 2019). Connecting the presence of LWC with lenticular clouds and icing events, Merino et al. (2019) evaluated the LWC simulated by WRF against measurements in the cloud. Their POD (0.56) and

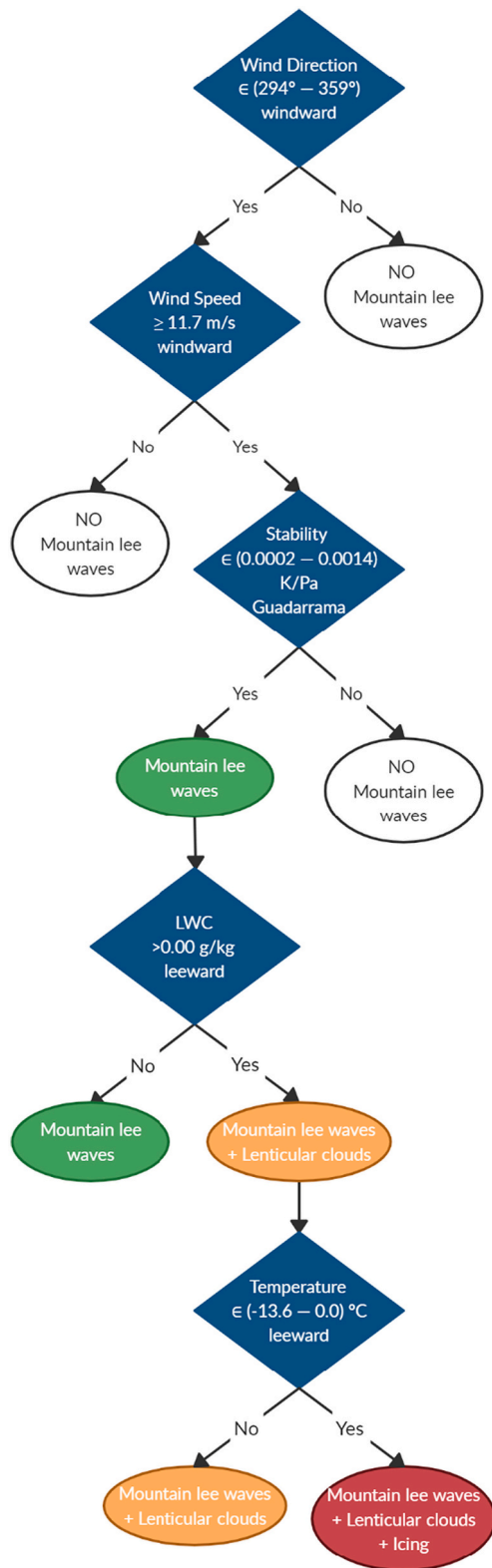


**Fig. 10.** HARMONIE decision tree for mountain lee waves, lenticular clouds and icing risk warning.

FAR (0.05) results are similar to those here presented. Moreover, Bolgiani et al. (2018) reported an aircraft icing event between 16:00 and 17:00 UTC on 28 February 2017 south-west of the Guadarrama mountains. This episode was validated using the icing warning from the decision tree and it was correctly forecasted by the WRF as well as the

HARMONIE NWP in the current study.

According to Wang and Lin (2000) and Muccilli (2015), another way to study the formation of mountain lee waves is via the Froude number ( $Fr$ ). The  $Fr$  threshold is usually fixed in  $Fr = 1$ , so that the flux may overpass the orographic barrier if  $Fr \geq 1$ , and on the contrary, the flux is blocked if  $Fr < 1$  (Carruthers and Hunt, 1990; Wang and Lin, 2000). Nonetheless, other studies (Smolarkiewicz and Rotunno, 1989; Smith, 2004; Navia-Osorio, 2012) demonstrated the possibility of mountain lee waves formation with  $Fr$  values between 0.5 and 1. Here,  $Fr$  is calculated windward of the mountain range following the same methodology used with the single variables and its 10-percentiles from both WRF and HARMONIE are additionally derived. While the HARMONIE  $Fr$  value is 0.2, the  $Fr$ -10 percentile is 0.8 for WRF, being within the interval showed for the abovementioned authors. Lin and Wang (1996) state that the flow can be classified into several different regimes depending on several  $Fr$  intervals. In regime IV ( $0.3 \leq Fr \leq 0.6$ ), a wave blocking arises and then a wave breaking; in regime III ( $0.6 \leq Fr < 0.9$ ), a wave breaking occurs and then blocking it; in regime II ( $0.9 < Fr \leq 1.12$ ), wave breaking with no-blocking in the leeward appears and in regime I ( $Fr \geq 1.12$ ), there is flow without wave breaking and blocking. Here, from the WRF (HARMONIE)  $Fr$  results, the regime IV arises in the 0% (11%), III in the 15% (17%), II in the 23% (24%) and regime I in the 62% (34%) of lenticular clouds associated to mountain lee waves events. The skill scores have been also evaluated (not shown), but the results obtained do not present any substantial improvement from the ones in Table 3.

## 5. Summary and conclusions

A comparative BT analysis between WRF and HARMONIE NWP models is carried out and validated using MSG-SEVIR images. To conduct it, several mountain wave episodes in the vicinity of LEMD airport are selected. Moreover, a characterization of mountain wave episodes is performed for both NWP models assessing the probability density functions for wind direction, wind speed, ST, LWC and temperature in 120 grid points over the research area. Finally, a decision tree is developed using the atmospheric variables percentiles to provide a warning method to forecast mountain lee waves, lenticular clouds and icing events.

The major conclusions of this research can be summarized as follows:

- The skill scores from the BT analysis reveals that the HARMONIE NWP model presents the best performance when simulating the BT across the whole domain. Nevertheless, the WRF model simulates BTs closer to those observed in the lenticular clouds range (260–275 K), which could imply a better model configuration for this particular phenomenon. Overall, the HARMONIE overestimates (BIAS = 3.69) while the WRF underestimates (BIAS = -4.94) these temperatures.
- Regarding the characterization, both models have a similar behavior in the wind direction percentiles. However, the wind speed in WRF is higher than in HARMONIE, as seen in other studies (Carvalho et al., 2014; Rasheed et al., 2014). Related to LWC, The HARMONIE simulates greater amounts of LWC in values lesser than 0.6 g/kg. However, for greater LWC values, the WRF density is higher. Observing the percentiles, the WRF minimum temperature range is greater than the HARMONIE one. This difference may not be trivial, as stated in the following conclusion.
- The ST for both NWP models is very different. While HARMONIE simulates all the ST values around neutral stability (0 K/Pa) and slightly positive values, the results for WRF are between the instability and stability (-0.06 to 0.05 K/Pa). These ST differences may be due notable temperature disagreements between the models.
- Simulated soundings by HARMONIE and WRF are in agreement with the observed sounding in LEMD (in the leeward side). Obtaining R results for temperature, dew point and wind speed higher than 0.85.

**Table 3**

Validation results for the decision tree warnings for WRF and HARMONIE models. The skill scores calculated are: False Alarm Ratio (FAR), Probability of Detection (POD), BIAS and Percentage Correct (PC).

	WRF			HARMONIE		
	Mountain lee waves	Mountain lee waves+Lenticular clouds	Mountain lee waves+Lenticular clouds+Icing	Mountain lee waves	Mountain lee waves+Lenticular clouds	Mountain lee waves+Lenticular clouds+Icing
FAR	0.32	0.00	0.41	0.30	0.00	0.31
POD	0.78	0.63	0.59	0.59	0.59	0.65
BIAS	1.15	0.63	1.00	0.85	0.59	0.94
PC	0.73	0.83	0.77	0.70	0.82	0.82

- Based on the HARMONIE mountain lee waves characterization results, 80% of the events present wind direction between 294° to 359° and wind speed between 11.7 and 21.7 m/s in the windward side. ST covers from 0.0002 to 0.0014 K/Pa over the Guadarrama mountains. In the leeward side, the maximum LWC and the minimum temperature ranges must be considered from 0.00 to 0.72 g/kg and from −13.6 to −2.4 °C, respectively.
- Comparing the skill scores from the verification of the mountain lee waves, lenticular clouds and icing warning, WRF results are better for all skill scores in the mountain lee waves and lenticular clouds warnings, whereas HARMONIE performs better the icing warnings.

The authors think that the verification results for the mountain lee waves, lenticular clouds and icing warnings have been satisfactory. The implementation of this tool as an operational forecasting in the research area could be suitable, improving the forecast of lenticular clouds and icing associated to mountain lee waves south of the Guadarrama range, having a significant impact in the safety of aircraft operations near LEMD airport. Moreover, this research could be extended to other airports where mountain lee waves events are frequent.

In future related research, it would be interesting to implement the Thompson microphysics scheme (used in the current WRF set-up) in the HARMONIE model to compare the results. In this line, recent investigations (Engdahl et al., 2020a, 2020b) have implemented elements from the Thompson cloud microphysical scheme in the HARMONIE model, showing a slightly improvement in supercooled liquid water, snow and graupel from the default physics options.

### Declaration of Competing Interest

The authors declare that there are no conflicts of interest regarding the publication of this paper.

### Acknowledgements

This work was partially supported by research projects: PID2019-105306RB-I00, CGL2016-78702-C2-1-R and CGL2016-78702-C2-2-R (SAFEFLIGHT project), FEI-EU-17-16 and SPESMART AND SPESVALE (ECMWF Special Projects). J. Díaz-Fernández acknowledges the grant supported from the MINECO-FPI program (BES-2017).

## Appendix A. Dataset

Table A1. Mountain lee waves events selected to simulate with the WRF and HARMONIE models.

Mountain lee waves events (yyyymmdd)						
for the validation	for the characterization					for the warnings validation
20171110	20010131	20030131	20050215	20080304	20091109	20170228
20171202	20010201	20030202	20050330	20080323	20091130	20181102
20171209	20010228	20030227	20051127	20080327	20091203	20190127
20180102	20010309	20031101	20060101	20081124	20100109	20180119
20180126	20010330	20031122	20060102	20081205	20100130	20180321
20180203	20011113	20031229	20060221	20081210	20100131	20200207
20180312	20011226	20031230	20061121	20081211	20100206	
20181102	20020131	20031231	20061122	20090126	20100209	
20181106	20020207	20040103	20061206	20090127	20100211	
20181126	20021130	20040109	20070218	20090128	20100330	
20181214	20021204	20040229	20070319	20090208	20101101	
20190120	20030106	20041219	20071115	20090306	20101118	
20190127	20030119	20041228	20071210	20091106	20101121	
	20030130	20050125	20080204			

## References

- Aznar, R., Sotillo, M.G., Martín, M.L., Somot, S., Valero, F., 2010. Comparison of model and satellite-derived long-term precipitation databases over the Mediterranean basin: a general overview. *Atmos. Res.* 97, 170–184. <https://doi.org/10.1016/j.atmosres.2010.03.026>.
- Belo-Pereira, M., 2015. Comparison of in-flight aircraft icing algorithms based on ECMWF forecasts. *Meteorol. Appl.* 22, 705–715. <https://doi.org/10.1002/met.1505>.
- Bengtsson, L., Andrae, U., Aspelien, T., Batrak, Y., Calvo, J., de Rooy, W., Gleeson, E., Hansen-Sass, B., Homleid, M., Hortal, M., Ivarsson, K.-I., Lenderink, G., Niemelä, S., Nielsen, K.P., Onville, J., Rontu, L., Samuelsson, P., Muñoz, D.S., Subias, A., Koltzow, M.O., 2017. The HARMONIE-AROME Model Configuration in the ALADIN-HIRLAM NWP System. *Mon. Weather Rev.* 145 (5), 1919–1935. <https://doi.org/10.1175/MWR-D-16-0417.1>.
- Bluestein, H.B., 1992. *Synoptic-Dynamic Meteorology in Midlatitudes: Volume 1, Principles of Kinematics and Dynamics*.
- Bolgiani, P., Fernández-González, S., Martín, M.L., Valero, F., Merino, A., García-Ortega, E., Sánchez, J.L., 2018. Analysis and numerical simulation of an aircraft icing episode near Adolfo Suárez Madrid-Barajas International Airport. *Atmos. Res.* 200, 60–69. <https://doi.org/10.1016/j.atmosres.2017.10.001>.
- Bolgiani, P., Santos-Muñoz, D., Fernández-González, S., Sastre, M., Valero, F., Martín, M.L., 2020. Microburst detection with the WRF model: effective resolution and forecasting indices. *J. Geophys. Res. Atmos.* 125 (14) <https://doi.org/10.1029/2020JD032883>. In press.
- Bormann, N., Hernandez-Carrascal, A., Borde, R. Gis, Lutz, H.J., Otkin, J.A., Wanzong, S., 2014. Atmospheric motion vectors from model simulations. Part I: Methods and characterization as single-level estimates of wind. *J. Appl. Meteorol. Climatol.* 53, 47–64. <https://doi.org/10.1175/JAMC-D-12-0336.1>.



- Broutman, D., Rottman, J.W., Eckermann, S.D., Hurlburt, E.O., 2001. A hybrid method for wave propagation from a localized source, with application to mountain waves. *Q. J. R. Meteorol. Soc.* 127 (571), 129–146. <https://doi.org/10.1256/smsqj.57107>.
- Buck, 2000. Aircraft Icing Handbook. Saf. Educ. Publ. Unit New Zealand.
- Carruthers, D.J., Hunt, J.C.R., 1990. Fluid mechanics of airflow over hills: turbulence, fluxes, and waves in the boundary layer. *Atmospheric Processes over Complex Terrain*. [https://doi.org/10.1007/978-1-935704-25-6\\_5](https://doi.org/10.1007/978-1-935704-25-6_5). In press.
- Carvalho, D., Rocha, A., Gómez-Gesteira, M., Silva Santos, C., 2014. WRF wind simulation and wind energy production estimates forced by different reanalyses: Comparison with observed data for Portugal. *Appl. Energy* 117, 116–126. <https://doi.org/10.1016/j.apenergy.2013.12.001>.
- Chevallier, F., Kelly, G., 2002. Model clouds as seen from space: Comparison with geostationary imagery in the 11-mm window channel. *Mon. Weather Rev.* 130, 712–722.
- Combal, B., Noel, J., 2009. Projection of Meteosat Images into World Geodetic System WGS-84 Matching Spot-vegetation Grid. JRC Scientific and Technical Reports, pp. 9–10. Available online: [http://publications.jrc.ec.europa.eu/repository/bitstream/JRC52438/combal\\_noel\\_msg\\_final.pdf](http://publications.jrc.ec.europa.eu/repository/bitstream/JRC52438/combal_noel_msg_final.pdf) (accessed on 6 May 2021).
- Díaz-Fernández, J., Quitián-Hernández, L., Bolgiani, P., Santos-Muñoz, D., García-Gago, A., Fernández-González, S., Valero, F., Merino, A., García-Ortega, E., Sánchez, J.L., Sastre, M., Martín, M.L., 2020. Mountain waves analysis in the vicinity of the Madrid-Barajas airport using the WRF model. *Adv. Meteorol.* 2020 <https://doi.org/10.1155/2020/8871546>.
- Díaz-Fernández, J., Bolgiani, P., Santos-Muñoz, D., Sastre, M., Valero, F., Sebastián-Martín, L.I., Fernández-González, S., López, L., Martín, M.L., 2021. On the characterization of mountain waves and the development of a warning method for aviation safety using WRF forecast. *Atmos. Res.* 258 <https://doi.org/10.1016/j.atmosres.2021.105620>.
- Doyle, J.D., Durran, D.R., 2002. The dynamics of mountain-wave-induced rotors. *J. Atmos. Sci.* 59 (2), 186–201.
- Dudhia, J., 1989. Numerical study of convection observed during the Winter Monsoon Experiment using a mesoscale two-dimensional model. *J. Atmos. Sci.* 46 (20), 3077–3107. [https://doi.org/10.1175/1520-0469\(1989\)046<3077:NSOCOD>2.0.CO;2](https://doi.org/10.1175/1520-0469(1989)046<3077:NSOCOD>2.0.CO;2).
- Eick, D., 2014. Turbulence Related Accidents & Incidents. <https://ral.ucar.edu/sites/default/files/public/events/2014/turbulence-impact-mitigation-workshop-2/docs/eick-turbulencelatedaccidents.pdf>.
- Engdahl, B.J.K., Nygaard, B.E.K., Losnedal, V., Thompson, G., Bengtsson, L., 2020a. Effects of the ICE-T microphysics scheme in HARMONIE-AROME on estimated ICE loads on transmission lines. *Cold Reg. Sci. Technol.* 179, 103139. <https://doi.org/10.1016/j.coldregions.2020.103139>.
- Engdahl, B.J.K., Thompson, G., Bengtsson, L., 2020b. Improving the representation of supercooled liquid water in the HARMONIE-AROME weather forecast model. *Tellus Ser. A Dyn. Meteorol. Oceanogr.* 72 <https://doi.org/10.1080/16000870.2019.1697603>.
- European Union Aviation Safety Agency, 2019. Annual Safety Review 2019. <https://doi.org/10.2822/098259>.
- Evans, J.K., 2014. An updated examination of aviation accidents associated with turbulence, wind shear and thunderstorm. In: Technical Report AMA Report Number 14–14. Analytical Mechanics Associates, Inc.
- Federal Aviation Administration (FAA), 2016. Advisory circular 00-6B: Aviation weather. doi:afcs-800 ac 91–97.
- Fernández-González, S., Merino Suances, A., Bolgiani, P., 2019. Pronóstico de engastamiento y ondas de montaña mediante modelos mesoescalares orientado a mejorar la seguridad aérea. In: Sexto Simposio Nacional de Predicción “Memorial Antonio Mestre”. <https://doi.org/10.31978/639-19-010-0.273>.
- Fernández-González, S., Sánchez, J.L., Gascón, E., López, L., García-Ortega, E., Merino, A., 2014. Weather features associated with aircraft icing conditions: a case study. *Sci. World J.* 2014. <https://doi.org/10.1155/2014/279063>.
- Gencer, C., Aydogan, E.K., Karahan, G., 2010. An algorithm predicting upper level icing potential by fuzzy set theory and an application with this algorithm for Turkey. *Open Ind. Manuf. Eng. J.* 3 (1) <https://doi.org/10.2174/1874152501003010007>.
- Gent, R.W., Dant, N.P., Cansdale, J.T., 2000. Aircraft icing. *Philos. Trans. R. Soc. A Math. Phys. Eng. Sci.* <https://doi.org/10.1098/rsta.2000.0689>.
- Geresdi, I., Rasmussen, R., 2005. Freezing drizzle formation in stably stratified layer clouds. Part II: the role of giant nuclei and aerosol particle size distribution and solubility. *J. Atmos. Sci.* 62 (7), 2037–2057. <https://doi.org/10.1175/JAS3452.1>.
- Gill, P.G., 2014. Objective verification of World area forecast Centre clear air turbulence forecasts. *Meteorol. Appl.* 21 (1), 3–11. <https://doi.org/10.1002/met.1288>.
- Gultepe, I., Sharman, R., Williams, P.D., Zhou, B., Ellrod, G., Minnis, P., Trier, S., Griffin, S., Yum, S.S., Gharabaghi, B., Feltz, W., Temimi, M., Pu, Z., Storer, L.N., Kneringer, P., Weston, M.J., Chuang, H. Ya, Thobois, L., Dimri, A.P., Dietz, S.J., França, G.B., Almeida, M.V., Neto, F.L.A., 2019. A review of high impact weather for aviation meteorology. *Pure Appl. Geophys.* 176, 1869–1921. <https://doi.org/10.1007/s00024-019-02168-6>.
- Hersbach, H., Bell, B., Berrisford, P., Hirahara, S., Horányi, A., Muñoz-Sabater, J., Nicolas, J., Peubey, C., Radu, R., Schepers, D., Simmons, A., Soci, C., Abdalla, S., Abellan, X., Balsamo, G., Bechtold, P., Biavati, G., Bidlot, J., Bonavita, M., De Chiara, G., Dahlgren, P., Dee, D., Diamantakis, M., Dragani, R., Flemming, J., Forbes, R., Fuentes, M., Geer, A., Haimberger, L., Healy, S., Hogan, R.J., Hólm, E., Janisková, M., Keeley, S., Laloyaux, P., Lopez, P., Lupu, C., Radnoti, G., de Rosnay, P., Rozum, I., Vamborg, F., Villaume, S., Thépaut, J.N., 2020. The ERA5 global reanalysis. *Q. J. R. Meteorol. Soc.* 146 <https://doi.org/10.1002/qj.3803>.
- Hong, S.Y., Noh, Y., Dudhia, J., 2006. A new vertical diffusion package with an explicit treatment of entrainment processes. *Mon. Weather Rev.* 134 (9) <https://doi.org/10.1175/MWR3199.1>, 2318–2334.
- Huang, Y., Franklin, C.N., Siems, S.T., Manton, M.J., Chubb, T., Lock, A., Alexander, S., Klekociuk, A., 2015. Evaluation of boundary-layer cloud forecasts over the Southern Ocean in a limited-area numerical weather prediction system using in situ, spaceborne and ground-based observations. *Q. J. R. Meteorol. Soc.* 141 (691), 2259–2276. <https://doi.org/10.1002/qj.2519>.
- Huffman, G.J., Norman, G.A., 1988. The supercooled warm rain process and the specification of freezing precipitation. *Mon. Weather Rev.* 116 (11), 2172–2182. [https://doi.org/10.1175/1520-0493\(1988\)116<2172:TSWRPA>2.0.CO;2](https://doi.org/10.1175/1520-0493(1988)116<2172:TSWRPA>2.0.CO;2).
- Jankov, I., Grasso, L.D., Sengupta, M., Neiman, P.J., Zupanski, D., Zupanski, M., Lindsey, D., Hillger, D.W., Birkenheuer, D.L., Brummer, R., Yuan, H., 2011. An evaluation of five ARW-WRF microphysics schemes using synthetic GOES imagery for an atmospheric river event affecting the California coast. *J. Hydrometeorol.* 12 <https://doi.org/10.1175/2010JHM1282.1>.
- Jiménez, P.A., Dudhia, J., González-Rouco, J.F., Navarro, J., Montávez, J.P., García-Bustamante, E., 2012. A revised scheme for the WRF surface layer formulation. *Mon. Weather Rev.* 140 (3), 898–918. <https://doi.org/10.1175/MWR-D-11-00056.1>.
- Kim, J.H., Chun, H.Y., 2011. Statistics and possible sources of aviation turbulence over South Korea. *J. Appl. Meteorol. Climatol.* 50 (2), 311–324. [https://doi.org/10.1175/1520-0434\(1997\)012<0253:OFADOM>2.0.CO;2](https://doi.org/10.1175/1520-0434(1997)012<0253:OFADOM>2.0.CO;2).
- Klemp, J.B., Lilly, D.R., 1975. The dynamics of wave-induced downslope winds. *J. Atmos. Sci.* 32 (2), 320–339.
- Koch, S.E., O’Handley, C., 1997. Operational forecasting and detection of mesoscale gravity waves. *Weather Forecast.* 12, 253–281. [https://doi.org/10.1175/1520-0434\(1997\)012<0253:OFADOM>2.0.CO;2](https://doi.org/10.1175/1520-0434(1997)012<0253:OFADOM>2.0.CO;2).
- Kunz, M., 2007. The skill of convective parameters and indices to predict isolated and severe thunderstorms. *Nat. Hazards Earth Syst. Sci.* 7, 327–342. <https://doi.org/10.5194/nhess-7-327-2007>.
- Ledesma, M., Baleraio, G., 2007. Meteorología aplicada a la aviación. Paraninfo. 13th ed. Paracuellos del Jarama. ISBN: 9788428329422.
- Lensky, I.M., Rosenfeld, D., 2008. Clouds-Aerosols-Precipitation Satellite Analysis Tool (CAPSAT). *Atmos. Chem. Phys.* 8 (22), 6739–6753. <https://doi.org/10.5194/acp-8-6739-2008>.
- Lilly, D.K., 1978. Severe downslope windstorm and aircraft turbulence event induced by a mountain wave. *J. Atmos. Sci.* 35, 59–77.
- Lin, Y., 2007. Mesoscale Dynamics, 1st Edition. Cambridge University Press, Cambridge, UK. ISBN: 9780511619649.
- Lin, Y.L., Wang, T.A., 1996. Flow regimes and transient dynamics of two-dimensional stratified flow over an isolated mountain ridge. *J. Atmos. Sci.* 53 (1), 139–158.
- López, L., García-Ortega, E., Sánchez, J.L., 2007. A short-term forecast model for hail. *Atmos. Res.* 83 (2–4), 176–184. <https://doi.org/10.1016/j.atmosres.2005.10.014>.
- Merino, A., García-Ortega, E., Fernández-González, S., Díaz-Fernández, J., Quitián-Hernández, L., Martín, M.L., López, L., Marcos, J.L., Valero, F., Sánchez, J.L., 2019. Aircraft icing: in-cloud measurements and sensitivity to physical parameterizations. *Geophys. Res. Lett.* 46, 11559–11567. <https://doi.org/10.1029/2019GL084424>.
- Mlawer, E.J., Taubman, S.J., Brown, P.D., Iacono, M.J., Clough, S.A., 1997. Radiative transfer for inhomogeneous atmospheres: RRTM, a validated correlated-k model for the longwave. *J. Geophys. Res. Atmos.* 102 (D14), 16663–16682. <https://doi.org/10.1029/97jd00237>.
- Moran, J.M., 1999. Meteorology: The Atmosphere and the Science of Weather 5th ed. Prentice Hall, p. 628. ISBN: 9780023838415.
- Muccilli, M., 2015. Using the Froude number to improve orographic snow forecasts in the Green Mountains of Vermont. *East. Reg. Tech. Attach.* (2015–5), 43.
- Naud, C.M., Booth, J.F., Del Genio, A.D., 2014. Evaluation of ERA-Interim and MERRA cloudiness in the southern ocean. *J. Clim.* 27 (5), 2109–2124. <https://doi.org/10.1175/JCLI-D-13-00432.1>.
- Navia-Osorio, R.P., 2012. Caracterización de las ondas de montaña en situaciones de precipitación invernal. Doctoral dissertation. Universidad de León.
- NCEP (National Centers for Environmental Prediction)/National Weather Service/NOAA/U.S., 2015. Department of Commerce: NCEP GFS 0.25 Degree Global Forecast Grids Historical Archive, Research Data Archive at the National Center for Atmospheric Research, Computational and Information Systems Laboratory. <https://doi.org/10.5065/D65B8PWK> (accessed on 7 May 2021).
- Olofsson, B., Olsson, E., Andersson, S., Mårtensson, T., Mårtensson, E., 2003. A new algorithm to estimate aircraft icing in the HIRLAM model. *Meteorol. Appl.* 10 (2), 111–114. <https://doi.org/10.1017/S1350482703002020>.
- Otkin, J.A., Greenwald, T.J., Sieglaff, J., Huang, H.L., 2009. Validation of a large-scale simulated brightness temperature dataset using SEVIRI satellite observations. *J. Appl. Meteorol. Climatol.* 48, 1613–1626. <https://doi.org/10.1175/2009JAMC2142.1>.
- Quitián-Hernández, L., Bolgiani, P., Santos-muñoz, D., Sastre, M., Díaz-Fernández, J., González-alemán, J.J., Farrán, J.L., López, L., Valero, F., Martín, M.L., 2021. Analysis of the October 2014 subtropical cyclone using the WRF and the HARMONIE-AROME numerical models: assessment against observations. *Atmos. Res.* <https://doi.org/10.1016/j.atmosres.2021.105697>.
- Rasheed, A., Süld, J.K., Kvamsdal, T., 2014. A multiscale wind and power forecast system for wind farms. *Energy Procedia.* <https://doi.org/10.1016/j.egypro.2014.07.238>.
- Rauber, R.M., Tokay, A., 1991. An explanation for the existence of supercooled water at the top of cold clouds. *J. Atmos. Sci.* 48 (8), 1005–1023. [https://doi.org/10.1175/1520-0469\(1991\)048<1005:AEFTEO>2.0.CO;2](https://doi.org/10.1175/1520-0469(1991)048<1005:AEFTEO>2.0.CO;2).
- Regmi, R.P., Kitada, T., Dudhia, J., Maharjan, S., 2017. Large-Scale Gravity current over the Middle Hills of the Nepal Himalaya: Implications for Aircraft Accidents. *J. Appl. Meteorol. Climatol.* 56, 371–390. <https://doi.org/10.1175/JAMC-D-16-0073.1>.
- Rogers, D.C., 1993. Measurements of natural ice nuclei with a continuous flow diffusion chamber. *Atmos. Res.* [https://doi.org/10.1016/0169-8095\(93\)90004-8](https://doi.org/10.1016/0169-8095(93)90004-8).
- Román-Cascón, C., Yagüe, C., Steeneveld, G.J., Morales, G., Arrillaga, J.A., Sastre, M., Maqueda, G., 2019. Radiation and cloud-base lowering fog events: Observational

- analysis and evaluation of WRF and HARMONIE. *Atmos. Res.* 229 <https://doi.org/10.1016/j.atmosres.2019.06.018>.
- Saha, S., Moorthi, S., Pan, H., Wu, X., Wang, J., Nadiga, S., Tripp, P., Kistler, R., Woollen, J., Behringer, D., Liu, H., Stokes, D., Grumbine, R., Gayno, G., Wang, J., Hou, Y., Chuang, H., Juang, H.H., Sela, J., Iredell, M., Treadon, R., Kleist, D., Van Delst, P., Keyser, D., Derber, J., Ek, M., Meng, J., Wei, H., Yang, R., Lord, S., van den Dool, H., Kumar, A., Wang, W., Long, C., Chelliah, M., Xue, Y., Huang, B., Schemm, J., Ebisuzaki, W., Lin, R., Xie, P., Chen, M., Zhou, S., Higgins, W., Zou, C., Liu, Q., Chen, Y., Han, Y., Cucurull, L., Reynolds, R.W., Rutledge, G., Goldberg, M., 2010. NCEP climate Forecast System Reanalysis (CFSR) 6-hourly Products, January 1979 to December 2010, Research Data Archive at the National Center for Atmospheric Research. *Comput. Inform. Syst. Lab.* <https://doi.org/10.5065/D69K487J>. (accessed on 7 May 2021).
- Schmetz, J., Pili, P., Tjemkes, S., Just, D., Kerkmann, J., Rota, S., Ratier, A., 2002. An introduction to Meteosat Second Generation (MSG). *Bull. Am. Meteorol. Soc.* 83 (7), 977–992. [https://doi.org/10.1175/1520-0477\(2002\)083<0977:AITMSG>2.3.CO;2](https://doi.org/10.1175/1520-0477(2002)083<0977:AITMSG>2.3.CO;2).
- Schultz, P., Politovich, M.K., 1992. Toward the improvement of aircraft-icing forecasts for the Continental United States. *Weather Forecast.* 7 (3), 491–500. [https://doi.org/10.1175/1520-0434\(1992\)007<0491:ttioai>2.0.co;2](https://doi.org/10.1175/1520-0434(1992)007<0491:ttioai>2.0.co;2).
- Sharman, R.D., Trier, S.B., Lane, T.P., Doyle, J.D., 2012. Sources and dynamics of turbulence in the upper troposphere and lower stratosphere: a review. *Geophys. Res. Lett.* 39 (12).
- Sheridan, P., Vosper, S., 2012. High-resolution simulations of lee waves and downslope winds over the Sierra Nevada during T-REX IOP 6. *J. Appl. Meteorol. Climatol.* 51 (7), 1333–1352.
- Shi, X., Li, Y., Liu, J., Xiang, X., Liu, L., 2018. Simulation of FY-2D infrared brightness temperature and sensitivity analysis to the errors of WRF simulated cloud variables. *Sci. China Earth Sci.* 61. <https://doi.org/10.1007/s11430-017-9150-0>.
- Skamarock, W.C., Klemp, J.B., 2008. A time-split nonhydrostatic atmospheric model for weather research and forecasting applications. *J. Comput. Phys.* 227 (7), 3465–3485. <https://doi.org/10.1016/j.jcp.2007.01.037>.
- Smith, R.B., Skubis, S., Doyle, J.D., Broad, A.S., Kiemle, C., Volkert, H., 2002. Mountain waves over Mont Blanc: influence of a stagnant boundary layer. *J. Atmos. Sci.* 59 (13), 2073–2092.
- Smith, S.A., 2004. Observations and simulations of the 8 November 1999 MAP mountain wave case. *Q. J. R. Meteorol. Soc.* 130, 1305–1325.
- Smolarkiewicz, P.K., Rotunno, R., 1989. Low froude number flow past three-dimensional obstacles. part i: baroclinically generated Lee Vortices. *J. Atmos. Sci.* 46, 1154–1164.
- Storer, L.N., Williams, P.D., Gill, P.G., 2019. Aviation Turbulence: Dynamics, forecasting, and Response to climate Change. *Pure Appl. Geophys.* 176 (5), 2081–2095. <https://doi.org/10.1007/s00024-018-1822-0>.
- Tafferner, A., Hauf, T., Leifeld, C., Hafner, T., Leykauf, H., Voigt, U., 2003. ADWICE: Advanced diagnosis and warning system for aircraft icing environments. *Weather Forecast.* 18, 184–203. [https://doi.org/10.1175/1520-0434\(2003\)018<0184:AADAWS>2.0.CO;2](https://doi.org/10.1175/1520-0434(2003)018<0184:AADAWS>2.0.CO;2).
- Tewari, M., Chen, F., Wang, W., Dudhia, J., LeMone, M.A., Mitchell, K., Ek, M., Gayno, G., Wegiel, J., Cuenca, R.H., 2004. Implementation and verification of the unified noah land surface model in the WRF model. *Bull. Am. Meteorol. Soc.* 2165–2170.
- Thompson, G., Brientjes, R.T., Brown, B.G., Hage, F., 1997. Intercomparison of in-flight icing algorithms. Part I: WISP94 real-time icing prediction and evaluation program. *Weather Forecast.* 12 (4), 878–889. [https://doi.org/10.1175/1520-0434\(1997\)012<0878:IOIFIA>2.0.CO;2](https://doi.org/10.1175/1520-0434(1997)012<0878:IOIFIA>2.0.CO;2).
- Thompson, G., Field, P.R., Rasmussen, R.M., Hall, W.D., 2008. Explicit forecasts of winter precipitation using an improved bulk microphysics scheme. Part II: Implementation of a new snow parameterization. *Mon. Weather Rev.* 136 (12), 5095–5115. <https://doi.org/10.1175/2008MWR2387.1>.
- Thompson, G., Politovich, M.K., Rasmussen, R.M., 2017. A numerical weather model's ability to predict characteristics of aircraft icing environments. *Weather Forecast.* 32 (1), 207–221. <https://doi.org/10.1175/WAF-D-16-0125.1>.
- Toros, H., Kahraman, A., Tilev-Tanriover, S., Geertsema, G., Gerard, C.A.T.S., 2018. Simulating heavy precipitation with HARMONIE, HIRLAM and WRF-ARW: a flash flood case study in Istanbul, Turkey. *Avrupa Bilim Teknol. Derg.* 13, 1–12.
- Udina, M., Soler, M.R., Sol, O., 2017. A modeling study of a trapped lee-wave event over the Pyrénées. *Mon. Weather Rev.* 145 (1), 75–96.
- Udina, M., Bech, J., Gonzalez, S., Soler, M.R., Paci, A., Miró, J.R., Trapero, L., Donier, J. M., Douffet, T., Codina, B., Pineda, N., 2020. Multi-sensor observations of an elevated rotor during a mountain wave event in the Eastern Pyrenees. *Atmos. Res.* 234, 104698. <https://doi.org/10.1016/j.atmosres.2019.104698>.
- Varlas, G., Anagnostou, M.N., Spyrou, C., Papadopoulos, A., Kalogiros, J., Mentzafou, A., Michaelides, S., Baltas, E., Karymbalis, E., Katsafados, P., Mather, A.A., Stretch, D.D., Singleton, A.T., Reason, C.J.C., Coning, De, Estelle, Musyoki, Thiffulufhelwi, R., Murungweni, F.M., Baltaci, H., Toros, H., Kahraman, A., Tilev-Tanriover, S., Geertsema, G., Cats, G., Coning, De, Estelle, Gijben, Maseko, B., Van Hemert, L., De Coning, E., Forbes, G., Poolman, E.E., Bangira, T., Maathuis, B.H.P., Dube, T., Gara, T.W., Estelle, Poolman, Kimambo, O.N., Chikore, H., Gumbo, J.R., Chang, J. H.-W., Kong, S.S.K., Sentian, J., Dayou, J., Chee, F.-P., Maddox, R.A., Chappell, C.F., Hoxit, L.R., Du Plessis, L.A., Pontrelli, M.D., Bryan, G., Fritsch, J.M., Ziv, B., Dayan, U., Sharon, D., Jubach, R., Sezin Tokar, A., Simpson, L.A., Dyson, L.L., 2019. Heavy precipitation and flooding on 12–14 February 1996 over the summer rainfall regions of South Africa: Synoptic and isentropic analyses. *Meteorog. Atmos. Phys.* 8.
- Wang, P.K., 2010. *Physics and Dynamics of Clouds and Precipitation*. Cambridge University Press. <https://doi.org/10.1017/CBO9780511794285>.
- Wang, T.A., Lin, Y.L., 2000. Effects of shear and sharp gradients in static stability on two-dimensional flow over an isolated mountain ridge. *Meteorog. Atmos. Phys.* 75 (1), 69–99.
- Weston, M., Chaouch, N., Valappil, V., Temimi, M., Ek, M., Zheng, W., 2019. Assessment of the sensitivity to the thermal roughness length in Noah and Noah-MP land surface model using WRF in an arid region. *Pure Appl. Geophys.* <https://doi.org/10.1007/s00024-018-1901-2>.
- Wolff, J.K., Sharman, R.D., 2008. Climatology of upper-level turbulence over the contiguous United States. *J. Appl. Meteorol. Climatol.* 47 (8), 2198–2214. <https://doi.org/10.1175/2008JAMC1799.1>.
- World Meteorological Organization, 2005. *Aerodrome Reports and Forecast*.
- Young, J.A., 2003. *Static Stability*. University of Wisconsin, Madison, WI, USA. [https://curry.eas.gatech.edu/Courses/6140/ency/Chapter7/Ency\\_Atmos/Static\\_Stability.pdf](https://curry.eas.gatech.edu/Courses/6140/ency/Chapter7/Ency_Atmos/Static_Stability.pdf).
- Zhang, T., Zhao, C., Gong, C., Pu, Z., 2020. Simulation of wind speed based on different driving datasets and parameterization schemes near dunhuang wind farms in Northwest of China. *Atmosphere* 11 (6), 647.